



Detecting freeze–thaw damage degradation of sandstone with initial damage using NMR technology

Taoying Liu¹ · Chaoyang Zhang¹ · Jiangteng Li¹ · Keping Zhou¹ · Cao Ping¹

Received: 7 July 2020 / Accepted: 9 April 2021 / Published online: 17 April 2021
© Springer-Verlag GmbH Germany, part of Springer Nature 2021

Abstract

The nuclear magnetic resonance (NMR) technique was used to study freeze–thaw damage degradation of sandstone with initial damage. The initial damage was fabricated by preloading, and the pore structure was detected using the NMR technique. Porosity, T_2 spectrum distribution, and T_2 spectral area were obtained. The magnetic resonance imaging (MRI) technique was used to obtain two-dimensional pore distribution images. Combined with uniaxial compressive strength tests, the effects of initial damage and freeze–thaw cycles on the mechanical properties of rock were studied and the failure mode of rock was analyzed. The results show that in the first 20 cycles, the numbers of micropores ($d \leq 1 \mu\text{m}$) and mesopores ($1 \mu\text{m} < d \leq 10 \mu\text{m}$) both increased. As the number of cycles further increased, the porosity of the sample was mainly affected by micropores. When the initial damage level is 50% or lower, as the number of freeze–thaw cycles increases, the ability of sandstone to accommodate permanent strain before failure gradually weakens and then increases again after 40 cycles. When the initial damage level reaches 70% or higher, the ability to accommodate permanent strain continues to weaken. The strain produced by sandstone before elastic deformation is roughly positively correlated with the number of mesopores and macropores in the sandstone. Under loading, the sandstone presents four failure modes: splitting failure, single shear failure, cone failure, and multi-crack failure.

Keywords Nuclear magnetic resonance technique · Initial damage · Freeze · thaw cycles · Mechanical property · Failure mode

Introduction

In China, transportation has always been a focus of national attention as it is the bottleneck of regional economic development. In recent years, the emergence of high-speed rail has effectively promoted regional economic development; however, the ultra-high driving speed creates high demands on the construction of transportation facilities. In cold regions, the safety and stability of roadbeds, tunnels, and other projects are seriously affected by freezing and thawing (Liu et al. 2019a; Mimouni et al. 2014), which limit high-speed railway speeds and require expensive engineering stability monitoring. Therefore, rail transit development requires an understanding of the freeze–thaw damage and deterioration characteristics of rock in cold regions for proactive risk prevention.

Presently, most research on freeze–thaw damage degradation of rocks in cold regions is based on the volume expansion theory; that is, the volume of water will increase by about 9% after freezing into ice, and the stress generated by the phase transition will lead to fracture expansion and rock property degradation (Bridgman 1912; Jia 2016; Liu et al. 2020; Zhou et al. 2018b; Gao et al. 2020). Many experiments have been conducted to study freeze–thaw damage and deterioration characteristics under different conditions (Al-Omari et al. 2014; Li et al. 2018b; Li et al. 2018a). The results indicate that freezing mode (Özbek 2014), freeze–thaw cycle environment (Zhang et al. 2019a; Deng et al. 2014; Yang et al. 2003), and lithology (Zhou et al. 2013; Wen et al. 2014) can greatly impact the damage and deterioration of rock. At the same time, many detection methods were also used by researchers to reveal the microscopic to macroscopic rupture process inside the sample during freeze–thaw cycles. Martínez-Martínez et al. (2013) used the scanning electron microscope to study the microstructure evolution of polished samples after freeze–thaw cycles. De Kock et al. (2015) and Liu et al. (2007) used CT technology to obtain the internal microstructure of the rock sample during the freeze–thaw process. Liu et al.

✉ Taoying Liu
taoying@csu.edu.cn

¹ School of Resources & Safety Engineering, Central South University, Changsha 410083, Hunan, China

(2019b) and Gao et al. (2019) studied the pore change characteristics of concrete and yellow sandstone by using nuclear magnetic resonance (NMR) technology, respectively. Among these technologies, NMR technology is only sensitive to the fluid medium in the rock pore, allowing for the detection of the internal structure of a material without destroying the measured object. The accompanying magnetic resonance imaging (MRI) technology can obtain high-resolution, two-dimensional images of the pore structure within the rock. Presently, NMR technology is a new means of physical performance analysis (Zhou et al. 2018a; Li 2012). Additionally, the internal structure of the rock has obvious control over its mechanical failure mode, so the internal damage can be analyzed qualitatively by correlating the failure mode of the rock sample with its damage characteristics (Liu and Cao 2017; Duan et al. 2019; Liu et al. 2015a).

Many experimental and theoretical studies on freeze–thaw damage characteristics of rock have been conducted. Yavuz (2011) tested the physical and mechanical properties of andesite samples after different freeze–thaw cycles and found that the P wave velocity, Schmidt hardness, and compressive strength decreased with freeze–thaw, while the porosity and water absorption showed the opposite trend. Bayram (2012) conducted freeze–thaw tests on several different limestone samples and, based on the test results, established a statistical model that can predict mechanical strength loss of natural stones after freeze–thaw. Tan et al. (2011) studied degradation of the mechanical properties of granite as a function of freeze–thaw cycles by uniaxial and triaxial compressive strength testing. Although they provide many valuable conclusions to elucidate freeze–thaw damage characteristics of rocks, most of the above studies focused on intact rock. In fact, initial damage is a key issue to be considered when conducting freeze–thaw mechanics research, for the following reasons: (1) Excavation of rock mass such as slopes and tunnels mainly adopts mining or mechanical rock breaking methods. The blasting vibration, mechanical disturbance, and unloading effects caused by excavation will inevitably damage the project; damage levels vary according to distance from the excavation surface (Wang et al. 2016b; Zhang et al. 2015). (2) Freezing and thawing mainly affect macroscopic mechanical properties by changing the internal structure of rock (Jiang 2018; Park et al. 2015). Initial damage inevitably aggravates the effects of freezing and thawing. (3) The initial damage is equivalent to the structural weak plane in the rock. The rock is disintegrated along the structural weak plane under loading, and initial damage changes the rock failure mode. Therefore, studying degradation characteristics of freeze–thaw damage with consideration of existing damage inside the rock is more suitable for practical engineering

conditions, and the results will be more practical for evaluating the engineering safety.

In view of the above reasons, studying the freeze–thaw damage degradation of rock while considering its internal initial damage, the test conditions are closer to actual engineering conditions. Compared with previous research results, the research conclusions will be more applicable and can effectively reduce the errors in safety assessment of engineering projects such as slopes and tunnels in cold regions. In this study, sandstone containing different initial damage levels were taken as the research object, and nuclear magnetic resonance technique and magnetic resonance imaging technique were used to track and monitor the changes of internal microstructure of samples during freeze–thaw process, which allows the mechanism of freeze–thaw damage to be analyzed from a microscopic perspective. A uniaxial compressive strength test was conducted on samples that had completed the target number of freeze–thaw cycles. The effects of the number of freeze–thaw cycles and the level of initial damage to the mechanical properties of rock, such as strength and deformation, were analyzed and the rock failure modes were summarized and analyzed. The research results can be used to evaluate the stability of sandstone slopes and tunnels, and predict their failure modes.

Experimental scheme

Sample preparation

Samples are Ordovician fine-grained red sandstone from Wuding, Yunnan province, with a particle size of 0.01–0.05 mm, whose physical and mechanical parameters are shown in Table 1. In order to minimize differences between samples and ensure comparability of experimental data, all samples were taken from the same rock block which was about 5 m below the surface. As per the international standard of rock mechanics (ISRM) (Bieniawski and Bernede 1979), the samples were cored to cylinders with a height of 100 mm and a diameter of 50 mm and the height and diameter error was less than 0.3 mm. In this study, in order to obtain more reliable test results, a group of 3 samples is designed for each test, resulting in 17 groups. One group was used to determine the ultimate UCS and 16 groups for 4 levels of initial damages (0%, 30%, 50%, and 70% of the ultimate UCS) and 4 numbers of freeze–thaw cycles (0, 20, 40, and 60). Finally, a total of 51 samples were used in the test.

Test steps

The test process consisted of the freeze–thaw cycle test, NMR detection, and uniaxial compressive strength test. The specific steps are as follows:

Table 1 Physical and mechanical parameters of sandstone

Type	Density (kg/m ³)	UCS (MPa)	Elasticity modulus (GPa)	Poisson’s ratio	Porosity (%)	LWV (m/s)
Red sandstone	2440	66.12	4.053	0.34	4.69	3145

UCS uniaxial compressive strength of sandstone, LWV longitudinal wave velocity

- (1) First, three rock samples were randomly selected from the samples for the uniaxial compressive strength test. The average value of their strength was considered the ultimate compressive strength. As shown in Table 2, the remaining samples randomly divided in four groups were subjected to loads equivalent to 0, 30, 50, and 70% of the ultimate compressive strength to create different levels of initial damage.
- (2) Since the magnetic field mainly resonates with H⁺ in H₂O, the pores inside the sample need to be filled with water before measuring the NMR properties of the sample. The sample was placed in a vacuum saturated device and saturated with water under a vacuum pressure of 0.1 MPa for 6 h, then the sample was immersed in distilled water for 24 h to completely saturate the internal pores.
- (3) The height, diameter, and NMR properties of the saturated rock samples were measured. The results of NMR tests included porosity, T₂ spectrum distribution, T₂ spectral area, and pore distribution images.
- (4) After the NMR test, samples were placed in a freeze–thaw testing machine. Considering that the average temperature of the coldest month in cold regions of China is around – 20 °C (Shen, 2016), and the room temperature is conventionally considered to be 20 °C, according to the Chinese regulation “Specifications for rock tests in water conservancy and hydroelectric engineering” (SL264-2001), which specifies that “the three saturated samples to put in a tin box, to freeze under -20±2°C for 4 hour, then immerse the box into water to thaw at 20±2°C for 4 hour to constitute a freeze-thaw cycle,” therefore, the temperature range of the testing machine was set at – 20~20 °C. Shen et al. (2016) found that for hard rocks with porosity less than 10%, when the cooling or heating time was 1 h, the sample reached a completely frozen or completely melted state. Therefore, each freeze–thaw cycle consisted of 4 h for freezing, 4 h for thawing, and 1 h for each cooling and heating.
- (5) Steps (2) and (3) were performed on samples after the completion of the 20th, 40th, and 60th freeze–thaw cycles. Uniaxial compressive strength tests at a 0.5-MPa/s loading rate were conducted on rock samples that had been subjected to different numbers of freeze–thaw cycles (0, 20, 40, 60). The compressive strength of the samples was measured and their failure modes were observed.

A schematic illustrating the test procedure is shown in Fig. 1. Instruments used in the test included a vacuum saturation device of which the range is 0~0.1 MPa. In the freeze–thaw cycling test, freeze–thaw testing machine TDS-300 was applied, and this machine mainly includes a refrigeration system and an automatic water inlet system. In the cooling stage, the refrigeration system is used to cool the air inside the testing machine, while in the heating stage, the automatic water inlet system will inject water into the testing machine and use water as a medium to increase the internal temperature of the testing machine. The freezing temperature range of the testing machine is – 15 ~ – 40 °C, the thawing temperature range is + 15 ~ + 20 °C, and the maximum number of automatic freezing and thawing cycles is 999. The magnetic field strength of the NMR testing system is 0.3 T ± 0.05 T, and the RF pulse frequency range is 2~49.9 MHz. The maximum load of the loading control system is 2000 kN with a relative error of ± 0.5%. It is worth mentioning that when analyzing the change law of porosity and uniaxial compressive strength, the data used is the mean value of three samples. For the T₂ spectrum curve and the MRI imaging and stress–strain curve, each sample has a unique corresponding result. Considering that this research focuses on the analysis of the freeze–thaw damage law of sandstone with initial damage, only the sample whose porosity is closest to the average porosity of the three samples is selected for analysis in these parts.

Results and analyses

NMR properties

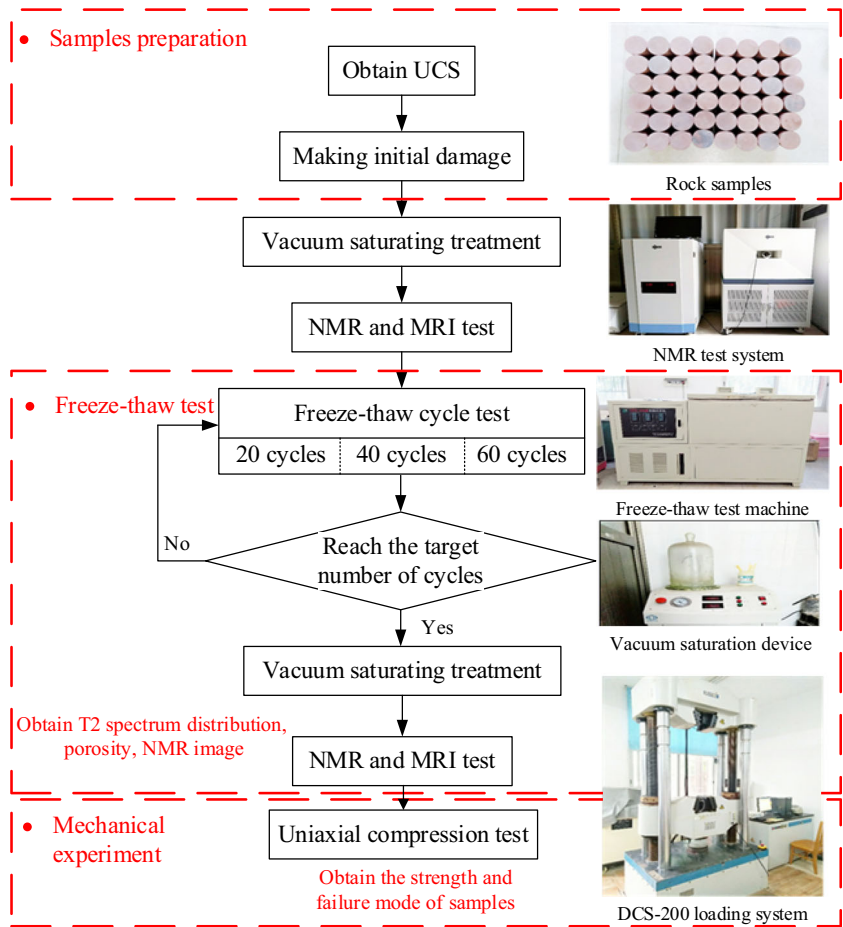
Introduction of the T₂ spectrum

Nuclear magnetic resonance refers to the nucleus response to radio frequency after magnetization by a magnetic field. By emitting a certain radio frequency (RF)

Table 2 Preload stress table (MPa)

Initial damage	0%	30%	50%	70%	UCS
Stress	0	19.84	33.06	46.28	66.12

Fig. 1 Test flow chart



pulse, NMR technology allows the hydrogen nuclei in the fluid medium within the porous rock to resonate and absorb the energy of the RF pulses. The hydrogen nucleus releases the absorbed energy when the RF pulse ends. Different pore sizes have different energy levels. Therefore, the pore distribution inside the rock can be determined by using a specific coil to detect energy released by the hydrogen nucleus (Li et al. 2019; Timur 1969).

Figure 2 shows the T_2 spectrum distribution obtained through inversion. The x -axis T_2 is the time constant of the transverse magnetization vector attenuation, which is called transverse relaxation time. It is caused by free relaxation, surface relaxation, and diffusion relaxation. This can be expressed as

$$1/T_2 = 1/T_{2\text{free}} + 1/T_{2\text{surface}} + 1/T_{2\text{diffusion}} \quad (1)$$

Free relaxation, $T_{2\text{free}}$, is the inherent liquid relaxation property, which is determined by physical properties such as viscosity and chemical composition of the liquid. Since the test samples in this test were saturated with water, the free relaxation of water is given by the following equation:

$$T_{2\text{free}} \approx 3(T_K/298\eta) \quad (2)$$

where T_K is the temperature in Kelvin, K, and η is the liquid viscosity in mPa·s.

Surface relaxation, $T_{2\text{surface}}$, occurs on the rock particle surfaces and is related to the specific surface area of the medium.

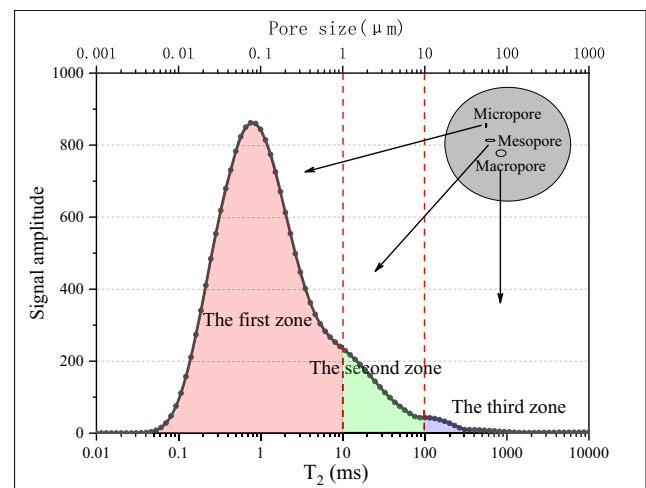


Fig. 2 T_2 spectrum distribution obtained through inversion

The larger the specific surface area, the more frequent the nuclear collisions and the shorter the relaxation time; thus, surface relaxation can be expressed as

$$T_{2\text{surface}} = \frac{1}{\rho_2(S/V)_{\text{pore}}} \tag{3}$$

where ρ_2 is the transverse relaxation strength of the rock surface, m/s, and $(S/V)_{\text{pore}}$ is the ratio of the pore surface area to the volume of fluid in the pore, m^{-1} .

When there is a significant gradient in the static magnetic field, the diffusion of molecules from one magnetic field to another will cause additional phase dispersion, affecting the relaxation rate. Diffusion relaxation, $T_{2\text{diffusion}}$, can be expressed as

$$T_{2\text{diffusion}} = \frac{12}{D(\gamma GT_E)^2} \tag{4}$$

where D is the diffusion coefficient, cm^2/s ; γ is the gyromagnetic ratio; G is the magnetic field gradient, Gs/cm ; and T_E is the echo time, ms.

Substituting Eqs. (2), (3), and (4) into Eq. (1) gives

$$\frac{1}{T_2} = \frac{298\eta}{3T_K} + \rho_2 \left(\frac{S}{V} \right)_{\text{pore}} + \frac{D(\gamma GT_E)^2}{12} \tag{5}$$

Because only water is contained in the pores and a short T_E is used for testing in the actual NMR process, the effects of free relaxation and diffusion relaxation on T_2 can be ignored, and T_2 is only related to the specific surface area of the pores. The larger the specific surface area, the shorter the relaxation time. The pore size is negatively correlated with the specific surface area; therefore, the larger the pore size, the larger the T_2 value. The y -axis of Fig. 2 represents the transverse magnetization vector strength, which is related to the number of hydrogen nuclei in the fluid medium. The spectral area enclosed by the curve and x -axis indicates the number of corresponding pores. The larger the spectral area, the greater the number of pores in the corresponding pore size range. In recent years, scholars have summarized a variety of pore size classification methods based on the test results of different rocks, but all of the existing classification methods are unsuitable for all types of rocks, and it is generally believed that lithologic differences have a great influence on the pore distribution in rocks. Considering that the sandstone used in this study is similar to the rock used by Lin et al. (2019), the T_2 spectrum curve can be divided into three zones, which represent pores with different sizes: micropores ($d \leq 1 \mu\text{m}$), mesopores ($1 \mu\text{m} < d \leq 10 \mu\text{m}$), and macropores ($d \geq 10 \mu\text{m}$).

Porosity

The essence of rock degradation under freeze–thaw cycles is that the fatigue load caused by initiation and dissipation of the

frost heaving force changes the pore structure inside the rock (Jia et al. 2017). Therefore, the variation of pores inside the rock during freeze–thaw cycles can directly reflect the evolution process of freeze–thaw damage.

Figure 3 shows the change in average porosity of sandstone with initial damage after different freeze–thaw cycles. The porosity of sandstone was observed to be affected by both the initial damage level as well as the number of freeze–thaw cycles. After preloading the samples with different axial loads, the porosity of the samples increased, indicating that initial damage occurred inside the samples. When the initial damage level is 50% or lower, the porosity of samples in the first 40 cycles increases continuously, while the 60th cycle shows a slight decrease. When the initial damage level is 70%, the growth trend of porosity is up, same and up. The porosity did not change significantly between 20 and 40 cycles. It is believed that after 40 freeze–thaw cycles, obvious damages such as particle shedding appeared on the sample surface (as shown in Fig. 4), and this phenomenon led to the low porosity. By observing the slope of the curve, it was determined that the effect of freeze–thaw on the internal structure of sandstone is obvious in the first 20 cycles, where the porosity increment is the largest. As the number of cycles increases, the slope of the curve begins to decrease, indicating that the freeze–thaw effect gradually weakens. On the other hand, when the initial damage level exceeds a certain threshold, the existence of initial damage can aggravate the damage degradation of sandstone. Therefore, when the initial damage level was 70%, the slope of the porosity curve increased again after 40 cycles.

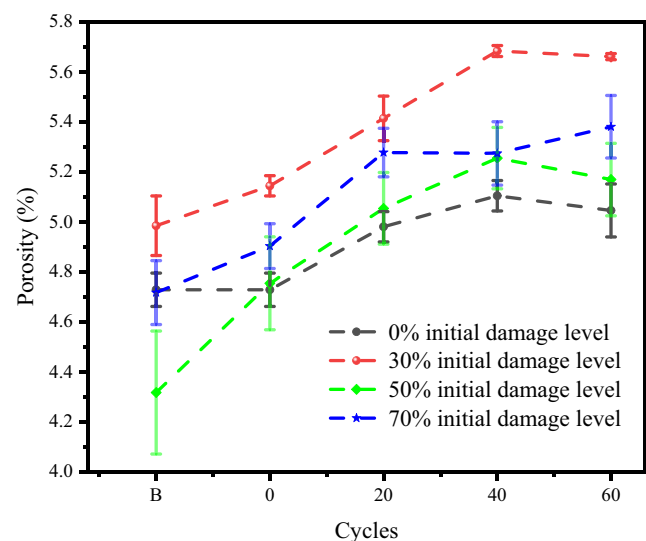


Fig. 3 Change in porosity of sandstone with initial damage during freeze–thaw cycles (B represents the porosity of the sample before preloading)

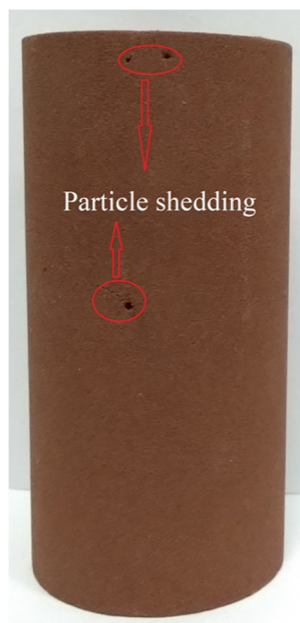


Fig. 4 The sample with 70% initial damage appeared to have particle shedding after 40 freeze–thaw cycles

T_2 spectrum distribution

The T_2 spectrum obtained by nuclear magnetic resonance technology reflects the pore distribution inside the rock. According to the principle of nuclear magnetic resonance technology, the T_2 value is positively correlated with the pore size and the signal amplitude is positively correlated with the number of pores of a corresponding pore size. Therefore, the pore changes in the rock can be understood through analyzing the T_2 spectrum obtained after different freeze–thaw cycles. Figure 5 shows the T_2 spectrum distribution curves of the three samples in the 70% test group before the initial damage, and it

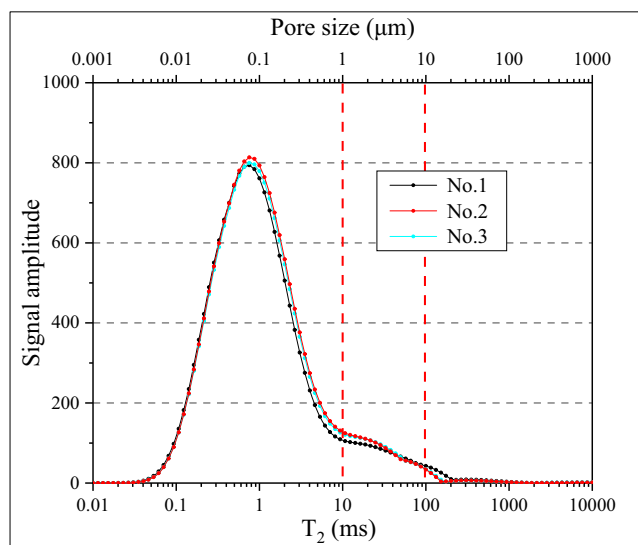


Fig. 5 T_2 spectrum distribution curves of the three samples in the 70% test group before the initial damage

can be found that the curves obtained by the three samples in the same group are relatively similar. In order to analyze the influence of freeze–thaw cycles and initial damage on the internal structure of sandstone, the T_2 spectrum curves obtained by each group are compared and analyzed in Fig. 6. Figure 6a–d shows the T_2 spectrum distribution of sandstone with different damage levels under freeze–thaw cycles. In these curves, the first zone is relatively large, while the other two zones are much smaller, indicating that there are more micropores in the sample, which is closely related to the particle size of the sandstone sample. According to the principle of NMR technology, the outward expansion of the curve indicates that the number of pores increases, and the right shift in the maximum T_2 value indicates the presence of larger pores within the sandstone. In Fig. 6a, the curve expands outwards after 20 freeze–thaw cycles, indicating that the freeze–thaw effect increases the number of pores inside the sandstone. In Fig. 6b, after the sample is subjected to a load equivalent to 30% of the ultimate UCS, the curve expands outwards in both the first and the second zones, indicating that the number of micropores and mesopores has increased, while the shrinkage of the curve in the third zone indicates that the prestress has closed part of the original macropores in the sample. Compared with the 40th cycle, the curve in the third zone is lower at the 60th cycle, indicating that a part of the macropores inside the sample is closed, and this is one of the reasons why the porosity decreases after 60 cycles. In Fig. 6c, when the initial damage level is 50%, compared with the 40th cycle, the curve in the first zone shrinks significantly after 60 cycles, while in Fig. 6d, when the initial damage level is 70%, the curve in the first zone expands obviously after 60 cycles, so their porosity change curves show different trends. By observing the second zone of the curve, it can be found that the sandstone with different levels of initial damage shows the same change trend. That is, the freeze–thaw effect causes the amplitude of the second zone to increase, but as the number of cycles continues to increase, the second zone does not change significantly, indicating that the first 20 freeze–thaw cycles have a significant influence on the number of mesopores in sandstone.

T_2 spectral area

The T_2 spectral area refers to the area of the closed region surrounded by the NMR T_2 spectrum curve and the x -axis; its size is proportional to the fluid volume inside the sample. When the rock sample is fully saturated, the T_2 spectral area can be used to characterize the number of pores inside the rock (Li et al. 2008). Therefore, analyzing the change in the T_2 spectral area can quantify the effects of freeze–thaw and initial damage on the internal microstructure of the rock. Table 3 lists the area of the T_2 zone in each group and its proportion in the total spectral area; in the table, the area of the first, second, and

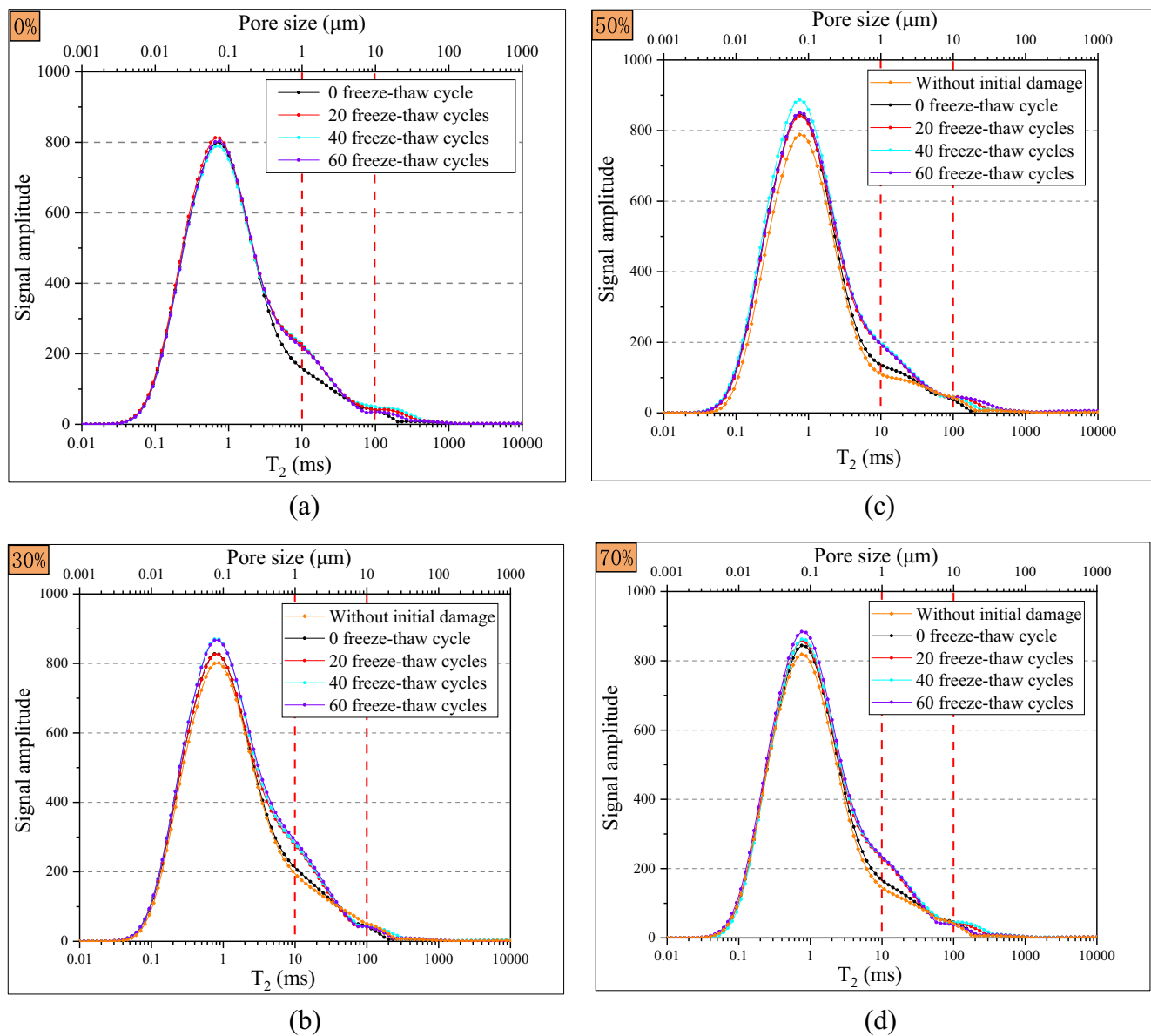


Fig. 6 T_2 spectrum distribution of sandstone with different initial damage levels under freeze–thaw cycles. **a** 0% initial damage level, **b** 30% initial damage level, **c** 50% initial damage level, **d** 70% initial damage level

third zones corresponds to the number of micropores, mesopores, and macropores, respectively.

By analyzing the data in Table 3, it can be found that during the freeze–thaw process, the variation trend of the zone area of the samples with initial damage levels of 0, 30, and 50% is the same. All manifested as the area of the first zone gradually increased as freeze–thaw cycles increased, but began to decrease after 40 cycles while the area of the second zone increased notably through the first 20 cycles. The area of the third zone was very low, indicating few macropores in the sample during the freeze–thaw cycles. When the initial damage level was 70%, the spectral area of the first and second zones increased in the first 20 cycles, indicating an increase in the number of micropores and mesopores. From 20 to 40

cycles, the spectral area changed little. After 40 cycles, the area of the first zone increased again while the area of the second zone decreased sharply. Analysis of the change in the T_2 spectral area suggests that the porosity increase after 40 cycles in the sample with 70% initial damage is mainly caused by rapid micropore initiation resulting from the action of the frost heaving force. As shown in Fig. 7, the rapid growth of the number of micropores in sandstone causes some mesopores and macropores to be squeezed into micropores, so that the number of micropores in the sample is larger and the distribution is more uniform at this stage. In addition, as shown in Fig. 8, the ends of the sample were severely peeled after 60 freeze–thaw cycles, and the pore information contained in the peeled part could not be collected, which also

Table 3 The area and proportion of the T_2 zone in each group

Initial damage	Cycles	Total spectral area	First zone	Second zone	Third zone	Proportion (%)		
						First zone	Second zone	Third zone
0%	0	17,808	17,722	73	13	99.52	0.41	0.07
	20	18,574	18,216	333	25	98.07	1.79	0.13
	40	19,044	18,673	353	18	98.05	1.85	0.09
	60	19,008	18,633	357	18	98.03	1.88	0.09
30%	W	18,436	18,326	78	32	99.40	0.42	0.17
	0	19,192	19,114	60	18	99.59	0.31	0.09
	20	20,090	19,774	240	76	98.43	1.19	0.38
	40	21,107	20,775	234	78	98.52	1.11	0.37
50%	60	21,022	20,652	333	37	98.24	1.58	0.18
	W	17,527	17,449	59	19	99.56	0.34	0.11
	0	18,127	18,033	80	14	99.48	0.44	0.08
	20	19,008	18,633	357	18	98.03	1.88	0.09
70%	40	19,958	19,572	366	20	98.07	1.83	0.10
	60	19,460	19,009	376	75	97.68	1.93	0.39
	W	17,970	17,895	58	17	99.58	0.32	0.09
	0	18,513	18,433	65	15	99.57	0.35	0.08
	20	19,724	19,305	398	21	97.88	2.02	0.11
	40	19,697	19,337	335	25	98.17	1.70	0.13
	60	20,278	20,182	80	16	99.53	0.39	0.08

W sample without initial damage

caused the area of the second zone and the third zone to be relatively small. In summary, in the first 20 cycles, the numbers of micropores and mesopores both increased, so the porosity of the sample increased significantly at this time, and the effect of the freeze–thaw cycles was obvious. With the further increase of the number of cycles, the change trend of the area of the first zone is the same as the change trend of the total spectral area; that is, the porosity occupied by micropores has the same change trend as the total porosity, so the porosity change of the sample is greatly affected by the micropores.

Moreover, the proportion of the three zones indicates that when the initial damage level is 50% or lower, for a same initial damage level, the zone proportions of the samples

subjected to 20, 40, and 60 freeze–thaw cycles are similar. At this time, the proportion changes of the first zone and the second zone are less than 0.4% and 0.5%, respectively. But they differ significantly from the zone ratio of the sample without the freeze–thaw cycle. When the initial damage level is 70%, from the 20th cycle to the 60th cycle, the proportion of the first zone increases by 1.65%, and the proportion of the second zone decreases by 1.63%, both of which are more than three times that of the other three damage levels. Therefore, it is apparent that the first 20 freeze–thaw cycles have caused obvious damage to the internal structure of sandstone, and when the initial damage level is 50% or lower, the number of freeze–thaw cycles has less impact on the damage effect.

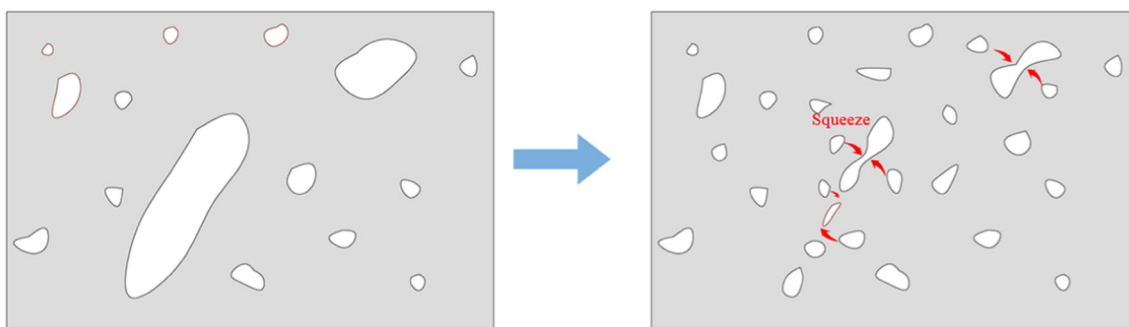


Fig. 7 Schematic diagram of micropores squeezing larger pores

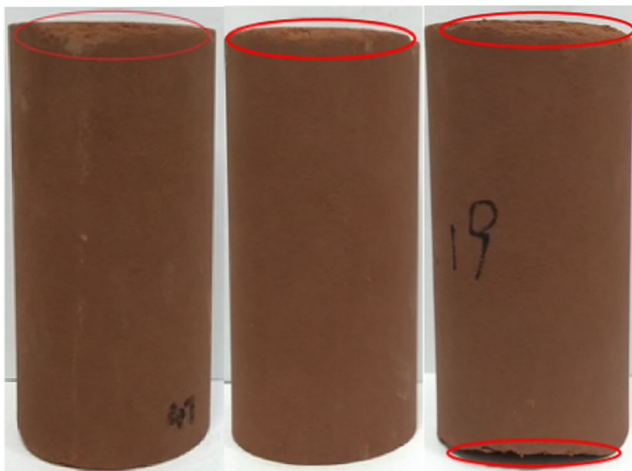


Fig. 8 The ends of the sample peeled off after 60 freeze–thaw cycles

When the initial damage level is higher than 50%, the internal structure of the sandstone is significantly damaged with the number of freeze–thaw cycles.

MRI results

MRI technology uses a gradient magnetic field to locate the signal released by the resonance between the hydrogen nucleus and the magnetic field, allowing the spatial distribution of the fluid medium inside the rock to be visually displayed (Jiang et al. 2019). In this study, MRI technology was used to analyze the internal structure of sandstone, and images of their pore distribution during freeze–thaw cycles were obtained. Figures 9, 10, 11, and 12, respectively, show the cross-sectional imaging results of sandstone with the four types of initial damage (0%, 30%, 50%, and 70% of the ultimate UCS) after different freeze–thaw cycles. In the image, the black area is the background color, and the bright spot is the detected signal, which represents the pores inside the sample. Therefore, the greater the number of bright spots, the more pores inside the sample. As shown in Fig. 13, the accumulation and expansion of pores into larger pores will lead to the aggregation of bright spots in some areas, thereby increasing

the brightness of the area. Thus, a larger brightness indicates a larger pore size.

As shown in Figs. 9a, 10 and 11a, before preloading, the bright spots are evenly distributed in the area, indicating that the sandstone particles are evenly distributed. Compared with the image before preloading, at 0 cycle, the image brightness increased under the action of compressive stress, which means that the prestress can cause obvious damage to the sample. At this time, when the prestress is 50% of the ultimate UCS, the sample has obvious pore accumulation at the two red circles as shown in Fig. 11b, and when the prestress was 70%, there are dense pores to the left of the red line in Fig. 12b. By observing Figs. 9, 10 and 11, it can be found that when the initial damage level is 50% or lower, the number of bright spots increases with the number of freeze–thaw cycles, indicating an increased number of pores in sandstone. After 40 freeze–thaw cycles, the bright spots at the edge of the image shown in Fig. 11d are more concentrated. Combined with the change of the T_2 spectrum curve in Fig. 6c, it can be found that the number of macropores in the sandstone with 50% initial damage decreases after 40 cycles, but at this time, some pores still expand into larger pores or micro-cracks. Figures 9d, 10e, and 11e show that compared with the 40th cycle, the number of spots inside the sample is slightly reduced after 60 cycles, indicating that a portion of the pores has been tightly closed by the application of the frost heaving force. As shown in Fig. 12a–e, when the initial damage level is 70%, the preload and 20 freeze–thaw cycles both increase the number of bright spots on the MRI image. Compared with the 20th cycle, the number of bright spots in the center of the image decreases after 40 cycles, but a relatively dense point domain appeared in the center right of the MRI image, indicating cracks in the sample. At this time, the total porosity of the sample changes very little. Different from the sample with an initial damage level of 50% or lower, after 60 freeze–thaw cycles, the bright spots inside the sample with 70% initial damage increase again and their distribution became more uniform, indicating even distribution of a large number of micropores in sandstone. In conclusion, the MRI results are consistent with the results obtained by analyzing the change of the T_2 spectral

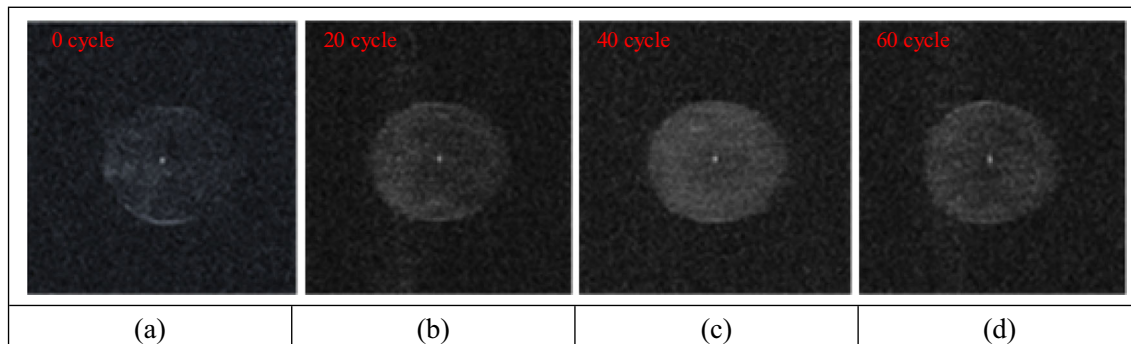


Fig. 9 a–d MRI results of sandstone without initial damage after different freeze–thaw cycles

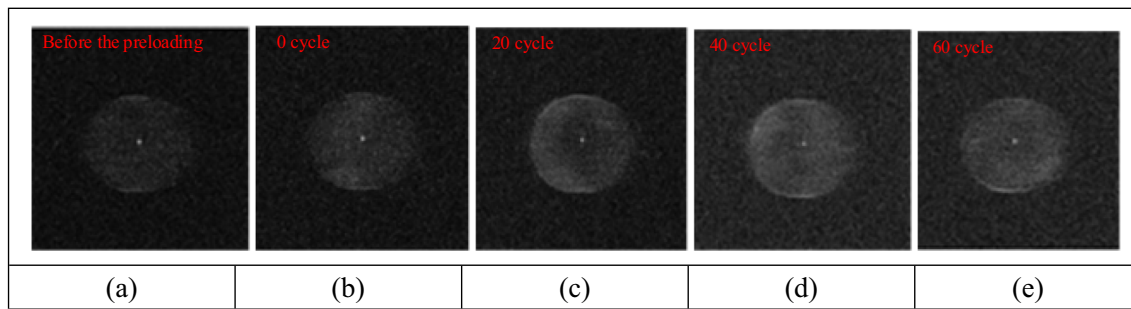


Fig. 10 a–e MRI results of sandstone with 30% initial damage after different freeze–thaw cycles

area. These images clearly reflect the structural characteristics of the pores in sandstone and provide reliable research data on the freeze–thaw damage characteristics of sandstone.

Results of uniaxial compressive strength tests

Uniaxial compressive stress

During freeze–thaw cycles, fatigue damage occurs to the rock due to repeated action of the frost heaving force (Liu et al. 2015b). The damage degradation of the sandstone by the freeze–thaw cycle is microscopically represented by changes to the pore distribution inside the rock, and macroscopically represented by the loss of mechanical strength of the rock. Uniaxial compressive tests were conducted on sandstone with different initial damage levels following the target freeze–thaw cycles. This was done to study the influence of the initial damage level and freeze–thaw cycle on mechanical strength, thus providing a basis for the safety and stability evaluation of projects. The uniaxial compressive strength values obtained in the study are listed in Table 4. Figure 14 shows the average uniaxial compressive strength of sandstone versus different levels of initial damage for different numbers of freeze–thaw cycles. With the same number of freeze–thaw cycles, sample strength decreases with increased initial damage levels. With 20 or 40 freeze–thaw cycles, the uniaxial compressive strength of the sample has a linear relationship with the initial damage level. With 60 freeze–thaw cycles, the decrease in value of the uniaxial compressive strength increases with the initial damage level. At this time, the decrease of uniaxial

compressive strength with an increasing initial damage level has a quadratic function relationship. Combined with the MRI results of Figs. 9, 10, 11 and 12, it is believed that when the initial damage level is low, the sandstone has relatively few damaged areas, and when the initial damage level is high, there are multiple damaged areas. Under the action of freeze–thaw cycles, the deterioration of these damaged areas is more serious, and these areas will also expand and penetrate first under load. Therefore, after 60 freeze–thaw cycles, these areas are severely damaged, which leads to multiple crack propagation in samples with higher level of initial damage. The crack path through the sample becomes shorter, and the premature failure leads to a significant decrease in the stress of the sample, so the stress change law changes.

In the figure, *A* and *B* represent the intensity reduction values of 40 cycles relative to 20 cycles and 60 cycles relative to 40 cycles, respectively. *A* is significantly greater than *B*, indicating that as the number of freeze–thaw cycles increases, the degradation effect of freeze–thaw cycles on the strength of sandstone gradually weakens. However, the overall strength reduction value is increasing, so the stability of sandstone is constantly weakening with the increase of the number of freeze–thaw cycles. Because the 20-cycle and 40-cycle fitting curves are parallel to each other, *A* remains the same for different levels of initial damage. As the initial damage level increases, *B* decreases first, then increases. Therefore, it can be concluded that the strength of sandstone decreases with the increase of the initial damage level and decreases as the number of freeze–thaw cycles increases. The degradation effect of freeze–thaw cycles on the uniaxial compressive strength of

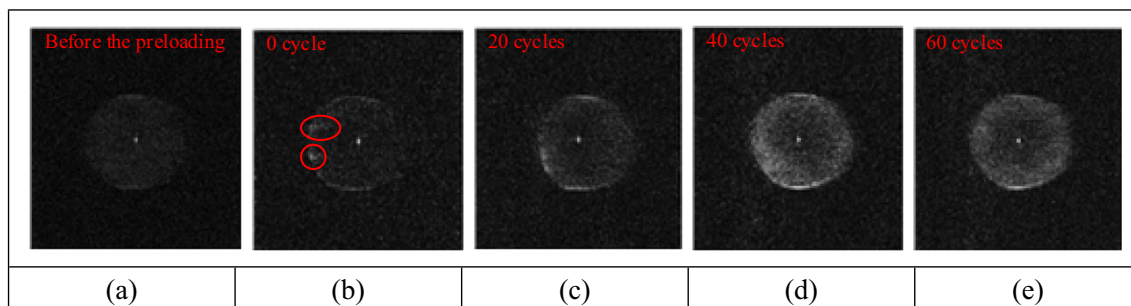


Fig. 11 a–e MRI results of sandstone with 50% initial damage after different freeze–thaw cycles

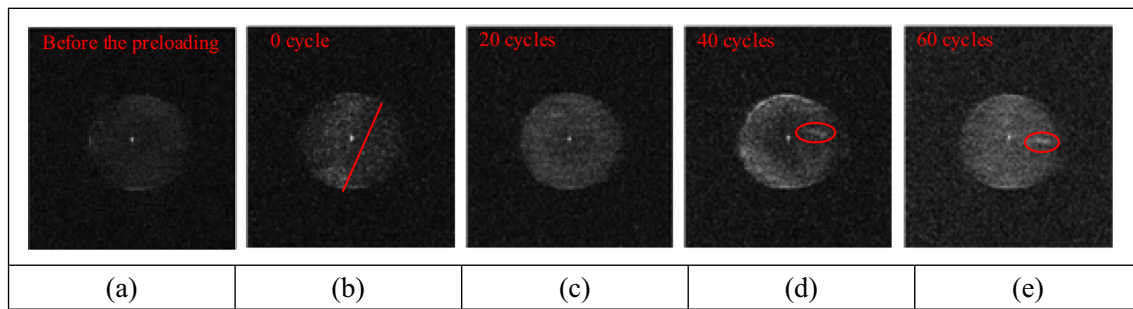


Fig. 12 a–e MRI results of sandstone with 70% initial damage after different freeze–thaw cycles

sandstone continues to weaken with the increase of the number of cycles, and the degradation effect is significantly weakened for rocks with 50% or lower initial damage. When the initial damage level is higher than 50%, the weakening gradually disappears as the level of damage increases.

Deformation characteristics

Figure 15 shows the stress–strain curve of sandstone sample without initial damage before freeze–thaw cycles, which can be roughly divided into five stages: the crack closure stage (OA), elastic stage (AB), stable cracking stage (BC), unstable cracking stage (CD), and post-peak stage (DE) (Kim et al. 2015). In the crack closure stage, the axial strain increases rapidly as the stress increases, and at this time, the pores and cracks in the sample caused by initial damage and freeze–thaw action are closed. In the elastic stage, there are fewer pores and cracks inside the sample. At this time, the strain increases linearly with the stress, and the deformation at this stage shows recoverable elastic deformation. With the further increase of the stress, the cracks inside the sample developed and expanded again, but the crack growth rate was slow, and the cracks would stop expanding when the load was removed. However, in the unstable cracking stage, excessive axial stress will cause the crack to expand and penetrate rapidly, and the small stress increment on the stress–strain curve can cause large deformation. When the loading stress reaches the ultimate compressive strength of the sandstone sample, the

sample begins to fail, that is, the post-peak stage. At this time, the axial stress decreases sharply with the failure of the sample.

Figure 16a–d shows the stress–strain curves of sandstone samples after 20, 40, and 60 freeze–thaw cycles at initial damage levels of 0, 30, 50, and 70%. According to the above analysis, the sample will produce irreversible ductile deformation in the “BD” segment. Therefore, the longer this segment is, the greater the ductile deformation of the sample will be. Observing Fig. 16a–c, it can be found that compared with the 20th cycle, when the number of freeze–thaw cycles is 40 times, the BD segment becomes shorter, and the sample experiences ductile–brittle transition. Here, “brittle” means that the ability of the sample to resist load decreases with permanent strain, and “ductile” means that the sample can accommodate permanent strain without losing the ability to resist load. With the continued increase of freeze–thaw cycles, the BD segment becomes longer after 60 cycles, and the sample undergoes brittle–ductile transition. In Fig. 16d, after 60 cycles, the sample fails after a small ductile deformation, and the stress decreases step-wise after failure. The main reason is that the sample with 70% initial damage already has serious damage after 60 cycles. Therefore, in the BD stage, the original micro-cracks can easily re-expand and cause premature failure of the sample.

Correlating the stress–strain curves in Fig. 16 with the T_2 spectrum area data in Table 3, it can be found that the length of the crack closure stage is roughly positively correlated with the number of mesopores and macropores in the sample,

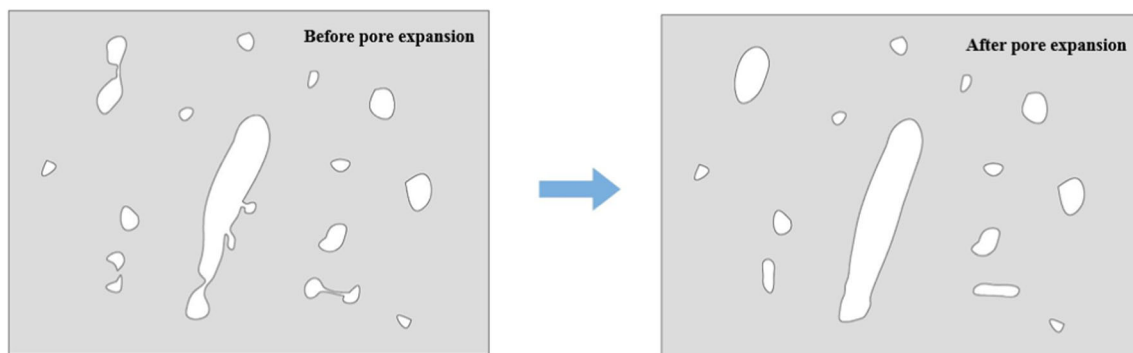


Fig. 13 Schematic diagram of small pores penetrating into larger pores

Table 4 UCS of sandstone versus different levels of initial damage for different numbers of freeze–thaw cycles (MPa)

Freeze–thaw cycles	Initial damage level			
	0%	30%	50%	70%
20	66.51	65.38	61.03	61.97
	65.72		62.72	55.78
	63.91		62.16	57.65
40	59.37	57.42	51.26	51.28
	54.78		51.38	48.99
	58.11		51.2	49.25
60	51.45	51.06	51.03	50.35
	53.26		48.78	47.76
	48.47		51.24	50.01
			48.39	43.24
				44.13
				37.84

which is characterized as the more pores with a size greater than 1 μm, the greater the strain of the sample during the crack closure stage. When the initial damage level is 70%, the spectral area corresponding to the mesopores and the macropores is small after 60 cycles, but a large strain occurs during the crack closure stage. The main reason is that the coupling of initial damage and long-term freeze–thaw cycles causes the rock particles to lose their cohesive force, so that the ends of the sample are severely peeled. The pore information contained in the peeled part cannot be collected, so the T_2 spectral area data is significantly smaller than other groups. In addition, the unevenness of the ends of the sample also leads to the large initial strain in the uniaxial compressive strength test.

In summary, when the initial damage level is 50% or lower, as the number of freeze–thaw cycles increases, the sandstone exhibits the deformation characteristics of ductile–brittle–ductile transition, and the turning point is around the 40th freeze–thaw cycle. When the initial damage level is 70%, the

brittleness of sandstone becomes more obvious with the increase of the number of freeze–thaw cycles. The strain in the crack closure stage of the stress–strain curve is roughly positively correlated with the number of mesopores and macropores in the sandstone.

Macroscopic failure modes

The macroscopic mechanical properties of rock materials comprehensively reflect the internal microstructure. Internal heterogeneity has an important influence on the macroscopic failure mode of brittle rock materials (Wang et al. 2006). The instability failure of rock samples is mainly caused by the expansion and penetration of the internal weak structural plane under the action of stress. Damage degradation can be analyzed according to the macroscopic fracture mode of the rock sample (Wang et al. 2016a). Figure 17 shows the failure modes of the three samples in the test group with 70% initial damage and 40 freeze–thaw cycles. Under load, the failure modes of the three samples with the same test conditions are

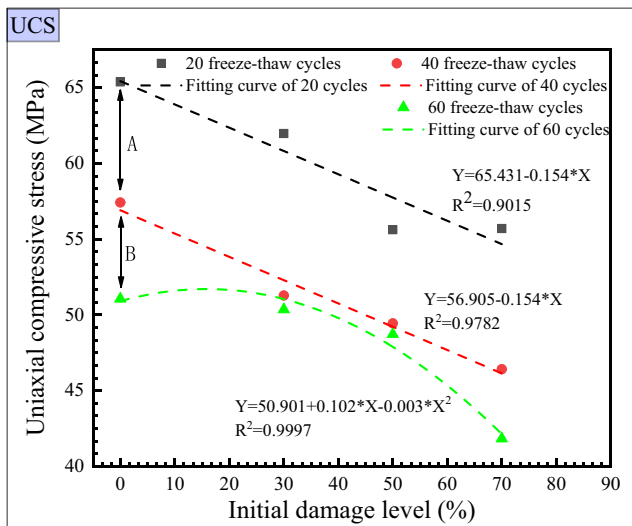


Fig. 14 UCS of sandstone versus different levels of initial damage for different numbers of freeze–thaw cycles

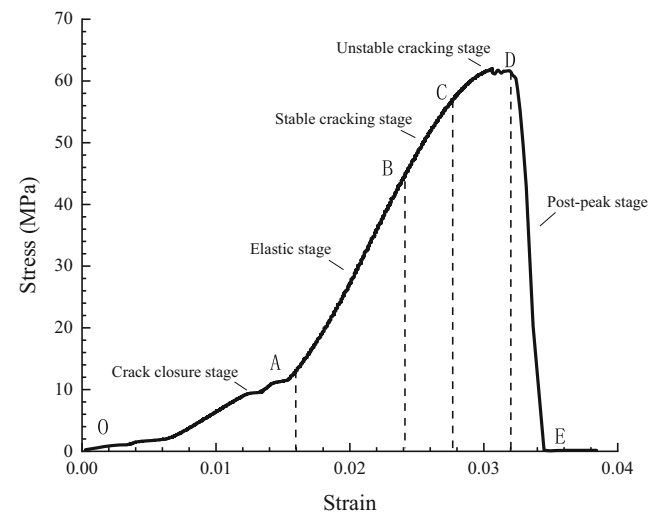


Fig. 15 Stress–strain curve of sandstone sample

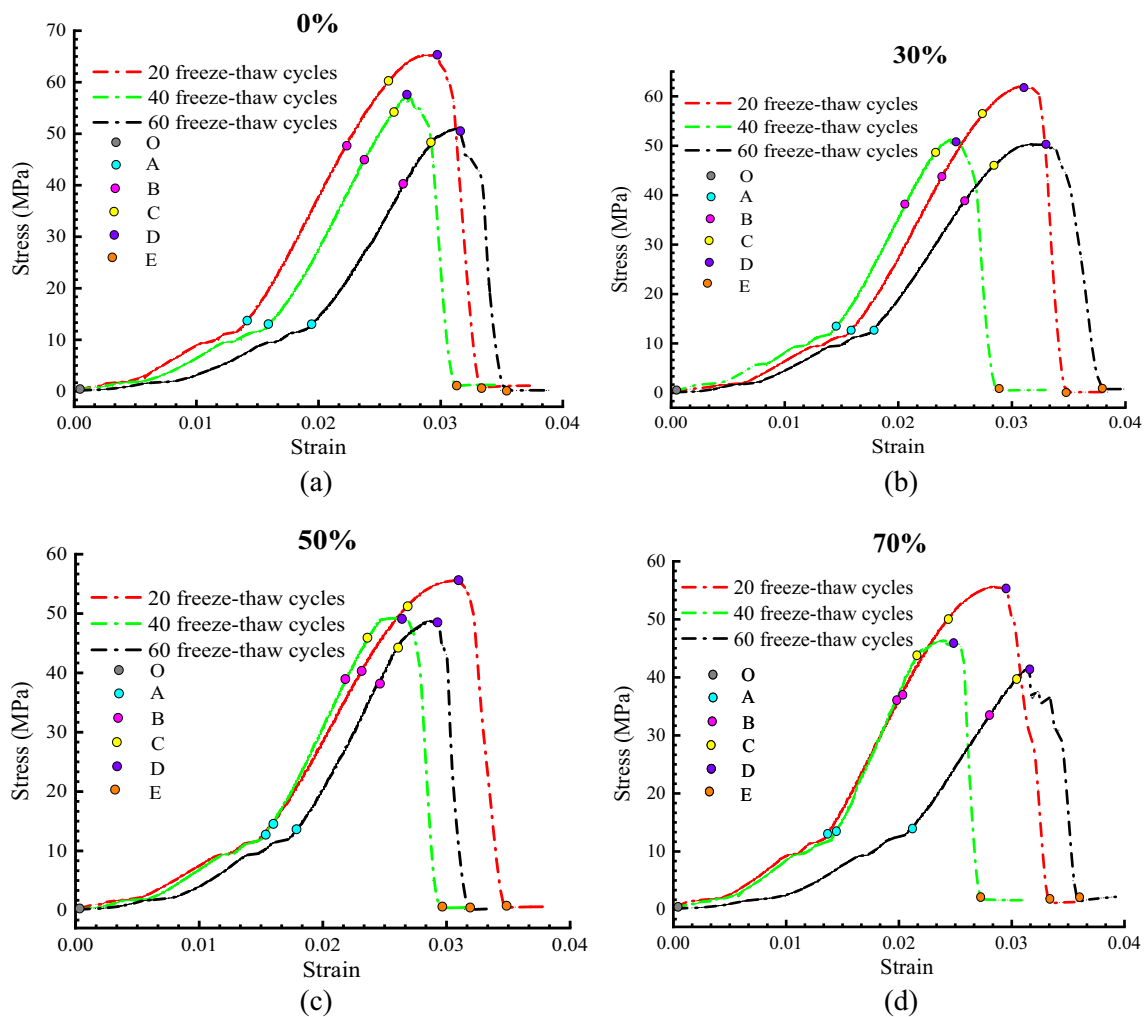


Fig. 16 Stress–strain curves of sandstone samples after 20, 40, and 60 freeze–thaw cycles at initial damage levels of 0 (a), 30 (b), 50 (c), and 70% (d) (OA, AB, BC, CD, and DE represent the crack closure stage,

elastic stage, stable cracking stage, unstable cracking stage, and post-peak stage, respectively.)

relatively similar, so one of them is placed in Fig. 18 to analyze the effect of initial damage and freeze–thaw cycles on the



Fig. 17 Failure modes of the three samples in the test group with 70% initial damage and 40 freeze–thaw cycles

failure modes of sandstone. Figure 18a–l shows the failure modes of sandstone with initial damage under different freeze–thaw cycles. In each frame, the left side shows a photograph of the broken rock, and the right side shows a corresponding sketch. The thickness of the line corresponds to the width of the crack.

By observing Fig. 18, it can be found that the macro failure of sandstone generally presents four modes under the influence of the freeze–thaw cycle and initial damage: splitting failure, single shear failure, cone failure, and multi-crack failure. Figure 18a–d shows that when the initial damage level is 0%, obvious tensile cracks appeared on the sample surface under loading, and shear cracks appear locally. At this time, the sample mainly undergoes splitting failure. With the increase of the initial damage level, shear cracks began to increase, and the failure mode of the sample tended to be complicated, with cone failure occurring at 70% damage level. By comparing Fig. 18a, e, and i, it can be found that without initial damage, as the number of freeze–thaw cycles increases, shear cracks began to appear near the ends of the

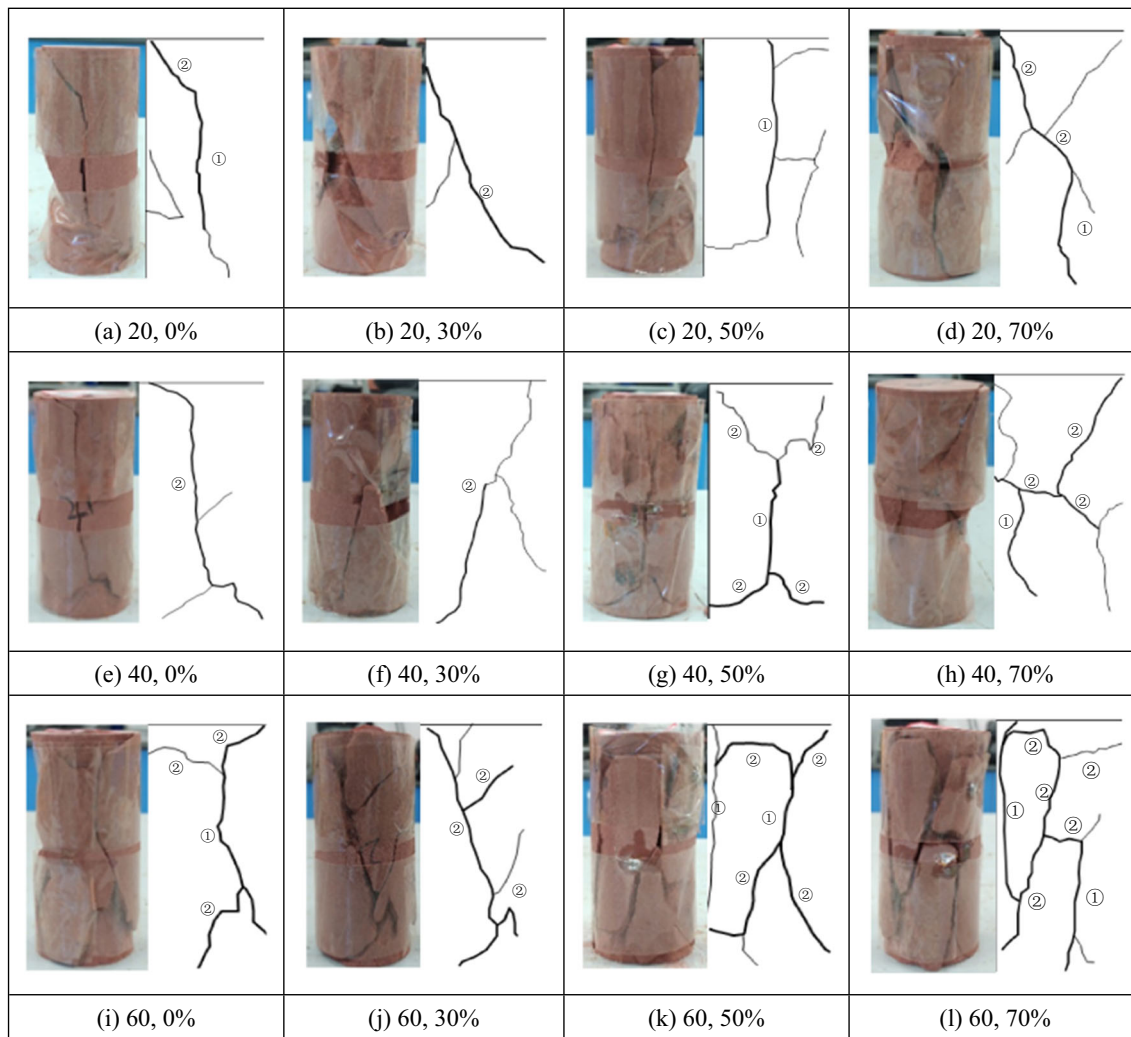


Fig. 18 Failure modes of samples with initial damage under different freeze–thaw cycles. (In the figure, “20” represents 20 cycles and “0%” represents 0% initial damage level; the left side of each frame is a photograph and the right side is a sketch with the thickness of the line

representing the width of the crack; ① represents tensile crack and ② represents shear crack.) **a** 20, 0%; **b** 20, 30%; **c** 20, 50%; **d** 20, 70%; **e** 40, 0%; **f** 40, 30%; **g** 40, 50%; **h** 40, 70%; **i** 60, 0%; **j** 60, 30%; **k** 60, 50%; **l** 60, 70%

sample, and the failure mode of the sample changed from splitting failure to shear failure and then to cone failure. After 40 freeze–thaw cycles, the sample showed a cone-shaped failure mode. At this time, shear cracks appeared near the two ends of the specimen and tapered bodies were cut at both ends, while tension cracks appeared between the two cones. Combined with the change of the T_2 spectrum area, it is believed that the reason for the change of the failure mode is that the number of mesopores and macropores increases under freezing and thawing conditions, and because there are more free surfaces at the end of the sample, the damage here is more serious during the freeze–thaw cycles, so shear cracks are prone to occur near the end under load. Observing the remaining figures, it can be found that with the increase of the initial damage and the number of freeze–thaw cycles, the failure mode of the sandstone has undergone the transformation of splitting failure–single shear failure–cone failure–multi-crack failure. The failure mode is becoming more

complicated, indicating that the internal damage of the sample is gradually serious. After 60 cycles, when the initial damage level was 50% or higher, the sample showed a multi-crack failure mode, indicating that there were already many structural weak planes inside the rock mass. In general, both freeze–thaw cycles and initial damage will increase shear cracks during sandstone failure. Under the coupling effect of the two, the failure mode of sandstone undergoes the transformation of splitting failure–single shear failure–cone failure–multi-crack failure, and the damage area gradually extends from the end to the center of the sample.

Discussion

In this study, NMR detection technology was used to detect the microstructure of sandstone with initial damage under

freeze–thaw cycles, and the quantitative analysis of the three types of pore changes inside the sandstone was realized. The study found that in the first 20 freeze–thaw cycles, the number of micropores and mesopores increased, and with the further increase of the number of cycles, the porosity occupied by micropores has the same change trend as the total porosity, and the porosity change of the sample is greatly affected by the micropores. This result shows that the freeze–thaw cycle causes general damage to sandstone by changing the number of micropores and mesopores in the sandstone. This is different from traditional excavation and blasting, which enable the rapid development of fractures in the rock while other parts are less affected. Therefore, the evaluation criteria such as fracture development level (only considering the fractures inside the rock mass and ignoring the microstructure damage of other parts) may have large deviations when evaluating the stability of freeze–thaw-damaged rock mass. On this basis, porosity should be taken as an auxiliary index to evaluate the engineering stability by measuring the porosity of collected samples or even the porosity of micropores and mesopores.

The uniaxial compressive test results show that before 40 cycles, as the initial damage level increases, the sample strength decreases linearly, and after 40 cycles, as the initial damage level increases, the sample strength decreases exponentially; that is, when the initial damage level is high, the sample strength will be severely deteriorated after 40 freeze–thaw cycles. Therefore, timely reinforcement of seriously damaged areas after excavation of slopes and other projects can effectively improve the durability of the project and reduce subsequent maintenance costs. In addition, this study found that with the increase of freeze–thaw cycles and initial damage, the shear cracks in the sample gradually increased, and the failure mode of sandstone undergoes the transformation of splitting failure–single shear failure–cone failure–multi-crack failure. Taking into account the common failure modes of slopes, it is believed that in the case of low initial damage and fewer freeze–thaw cycles, sandstone is mainly in the form of split failure. Therefore, in the early stage of slope formation, the slope is prone to collapse under the load on the top surface of the slope. At this time, for the developed cracks parallel to the slope surface, it is necessary to install anchor rods in the direction of vertical crack expansion for reinforcement. As the initial damage level increases and the number of freeze–thaw cycles increases, the shear cracks during sandstone failure increase, and the corresponding slopes are prone to translational sliding failure, wedge failure, or arc failure. At this time, it is necessary to stop the shear crack on the slope surface, while a retaining wall or other protective measures need to be built at the foot of the slope. When the initial damage level exceeds 50% or the number of freeze–thaw cycles is more than 60 times, the sandstone will be damaged by multiple cracks. Therefore, grouting reinforcement and shotcrete support are required for areas with serious damage or slopes with a long service life, and suspension of use if necessary.

However, due to the limitation of test conditions, only 60 cycles of freeze–thaw tests were carried out in this study, the damage to the rock structure caused by freeze–thaw was quite limited, so further research is needed. The study will also consider the following factors: different rock types, different freeze–thaw conditions, more freeze–thaw cycles, and the arrangement of the rock pore network. Otherwise, the faster the cooling rate, the faster the corresponding frost heave force growth rate, and the greater the final frost heave force (Zhang et al. 2019b). In the natural environment, the freeze–thaw cycle is a long-term process. However, in this study, the cooling rate is relatively fast, and the damage is stronger than the real situation, which is the shortcoming of this research. In future research, we will also try to use slow freeze–thaw method to reduce the influence of cooling rate on the test results.

Conclusions

In this study, NMR technology was used to evaluate the freeze–thaw damage degradation of sandstone with initial damage. During freeze–thaw cycles, changes to microstructural parameters such as porosity, T_2 spectrum distribution, and T_2 spectral area were obtained. Uniaxial compressive strength tests were conducted to analyze the strength deterioration law of sandstone, and the failure modes were summarized. This study reveals the freeze–thaw damage degradation characteristics of sandstone with initial damage.

- (1) When the initial damage level was 50% or lower, the porosity of samples in the first 40 cycles increased continuously, while the 60th cycle showed a slight decrease. The freeze–thaw effect was obvious on the internal structure of samples in the first 20 cycles and then gradually weakened. When the initial damage level was 70%, the slope of the porosity curve increased again after 40 cycles, indicating that the existence of an initial damage can aggravate the damage degradation of sandstone.
- (2) The results of the T_2 spectrum showed that in the first 20 cycles, the numbers of micropores ($d \leq 1 \mu\text{m}$) and mesopores ($1 \mu\text{m} < d \leq 10 \mu\text{m}$) both increased. Therefore, the porosity of the sample increased significantly at this time, and the effect of the freeze–thaw cycle was obvious. As the number of cycles further increased, the porosity of the sample was mainly affected by micropores, and when the initial damage level was 50% or lower, the number of freeze–thaw cycles had less impact on the damage effect. When the initial damage level was higher than 50%, the internal structure of the sandstone was significantly damaged with the number of freeze–thaw cycles.
- (3) The strength of sandstone decreases with the increase of the initial damage level and decreases as the number of freeze–thaw cycles increases. The degradation effect of freeze–

thaw cycles on the uniaxial compressive strength of sandstone continues to weaken with the increase of the number of cycles, and the degradation effect is significantly weakened for rocks with 50% or lower initial damage. When the initial damage level is higher than 50%, the weakening gradually disappears as the level of damage increases.

- (4) When the initial damage level is 50% or lower, as the number of freeze–thaw cycles increases, the sandstone exhibits the deformation characteristics of ductile–brittle–ductile transition, and the turning point is around the 40th freeze–thaw cycle. When the initial damage level is 70%, the brittleness of sandstone becomes more obvious with the increase of the number of freeze–thaw cycles. The strain in the crack closure stage of the stress–strain curve is roughly positively correlated with the number of mesopores and macropores ($d \geq 10 \mu\text{m}$) in the sandstone.
- (5) The macro failure of sandstone generally presents four modes: splitting failure, single shear failure, cone failure, and multi-crack failure. Both freeze–thaw cycles and initial damage will increase shear cracks during sandstone failure. Under the coupling effect of the two, the damage mode of sandstone undergoes the transformation of splitting failure–single shear failure–cone failure–multi-crack failure, and the damage area gradually extends from the end to the center of the sample.

In general, the internal structure and mechanical properties of sandstone have changed under the combined effect of initial damage and freeze–thaw cycles. When the initial damage level is 50% or lower, the existence of initial damage has relatively little influence on the freeze–thaw damage characteristics of sandstone. The freeze–thaw damage evolution laws of sandstone with initial damage and intact sandstone are similar, and both show that the freeze–thaw effect is obvious in the first 20 cycles and then gradually weakens. The influence of freeze–thaw cycles on the uniaxial compressive strength of the samples gradually weakens as the number of cycles increases, and the sandstone exhibits the deformation characteristics of ductile–brittle–ductile transition. When the initial damage level is 70% or higher, the evolution law of freeze–thaw damage changes significantly. The existence of initial damage causes serious damage to the internal structure of sandstone with the increase of the number of freeze–thaw cycles. The uniaxial compressive strength of sandstone has been greatly reduced with the freeze–thaw cycle, and its brittleness has become more obvious.

Acknowledgements This paper gets its funding from Project (51774323, 52004327), supported by the National Natural Science Foundation of China; Project (2018JJ3676), supported by the Natural Science Foundation of Hunan Province, China; Project (2018M643003), supported by China's Post-doctoral Science Fund; Project (2018YFC0808404), supported by the National Key Research and Development Program of China; and Project (2017zzts570), supported by graduate student

innovation plan of Central South University. The authors wish to acknowledge this support.

References

- Al-Omari A, Brunetaud X, Beck K, Al-Mukhtar M (2014) Effect of thermal stress, condensation and freezing–thawing action on the degradation of stones on the Castle of Chambord, France. *Environ Earth Sci* 71(9):3977–3989. <https://doi.org/10.1007/s12665-013-2782-4>
- Bayram F (2012) Predicting mechanical strength loss of natural stones after freeze–thaw in cold regions. *Cold Reg Sci Technol* 83–84:98–102. <https://doi.org/10.1016/j.coldregions.2012.07.003>
- Bieniawski ZT, Bernede MJ (1979) Suggested methods for determining the uniaxial compressive strength and deformability of rock materials: Part 1. Suggested method for determination of the uniaxial compressive strength of rock materials. *Int J Rock Mech Min Sci Geomech Abstr* 16(2):137. [https://doi.org/10.1016/0148-9062\(79\)91450-5](https://doi.org/10.1016/0148-9062(79)91450-5)
- Bridgman PW (1912) Water, in the liquid and five solid forms, under pressure. *Proc Am Acad Arts Sci* 47(13):441–558. <https://doi.org/10.2307/20022754>
- De Kock T, Boone MA, De Schryver T, Van Stappen J, Derluyn H, Masschaele B (2015) A pore-scale study of fracture dynamics in rock using x-ray micro-CT under ambient freeze–thaw cycling. *Environ Sci Technol* 49(5):2867–2874. <https://doi.org/10.1021/es505738d>
- Deng HW, Dong CF, Li JL, Zhou KP, Tian WG, Zhang J (2014) Experimental study on sandstone freezing–thawing damage properties under condition of water chemistry. *Appl Mech Mater* 608–609: 726–731. <https://doi.org/10.4028/www.scientific.net/AMM.608-609.726>
- Duan K, Li Y, Wang L, Zhao G, Wu W (2019) Dynamic responses and failure modes of stratified sedimentary rocks. *Int J Rock Mech Min Sci* 122:104060. <https://doi.org/10.1016/j.ijmms.2019.104060>
- Gao F, Xiong X, Zhou K, Li J, Shi W (2019) Strength deterioration model of saturated sandstone under freeze–thaw cycles. *Rock Soil Mech* 40(03):926–932. <https://doi.org/10.16285/j.rsm.2017.1886>
- Gao F, Cao S, Zhou K, Lin L, Zhu L (2020) Damage characteristics and energy-dissipation mechanism of frozen–thawed sandstone subjected to loading. *Cold Reg Sci Technol* 169:102920. <https://doi.org/10.1016/j.coldregions.2019.102920>
- Jia H (2016) Theoretical damage models of porous rocks and hard jointed rocks subjected to frost action and further experimental verifications. China University of Geosciences, Wuhan
- Jia H, Xiang W, Shen Y, Yang G (2017) Discussion of the key issues within calculation of the fatigue damage of rocks subjected to freeze–thaw cycles. *Chin J Rock Mech Eng* 36(2):335–346. <https://doi.org/10.13722/j.cnki.jjme.2016.0437>
- Jiang H (2018) The relationship between mechanical properties and gradual deterioration of microstructures of rock mass subject to freeze–thaw cycles. *Earth Sci Res J* 22(1):53–57. <https://doi.org/10.15446/esrj.v22n1.66108>
- Jiang Z, Deng H, Liu T, Tian G, Tang L (2019) Study on microstructural evolution of marble under cyclic dynamic impact based on NMR. *IEEE Access* 7:138043–138055. <https://doi.org/10.1109/ACCESS.2019.2935841>
- Kim J, Lee K, Cho W, Choi H, Cho G (2015) A comparative evaluation of stress–strain and acoustic emission methods for quantitative damage assessments of brittle rock. *Rock Mech Rock Eng* 48(2):495–508. <https://doi.org/10.1007/s00603-014-0590-0>
- Li J (2012) Experiment study on deterioration mechanism of rock under the conditions of freezing–thawing cycles in cold regions based on NMR technology. Central South University, Changsha

- Li H, Zhu J, Guo H (2008) Methods for calculating pore radius distribution in rock from NMR T2 spectra. *Chin J Magnetic Reson* 25(2): 273–280. <https://doi.org/10.3969/j.issn.1000-4556.2008.02.016>
- Li H, Li H, Wang K, Liu C (2018a) Effect of rock composition microstructure and pore characteristics on its rock mechanics properties. *Int J Min Sci Technol* 28(2):303–308. <https://doi.org/10.1016/j.ijmst.2017.12.008>
- Li J, Zhou K, Liu W, Zhang Y (2018b) Analysis of the effect of freeze–thaw cycles on the degradation of mechanical parameters and slope stability. *Bull Eng Geol Environ* 77(2):573–580. <https://doi.org/10.1007/s10064-017-1013-8>
- Li J, Kaunda RB, Zhu L, Zhou K, Gao F (2019) Experimental study of the pore structure deterioration of sandstones under freeze–thaw cycles and chemical erosion. *Adv Civil Eng* 2019:1–12. <https://doi.org/10.1155/2019/9687843>
- Lin Y, Zhou K, Gao F, Liu T, Liu C (2019) Experimental investigations on pore structure and mechanical properties of sandstone subjected to chemical corrosion. *IEEE Access*:1. <https://doi.org/10.1109/ACCESS.2019.2932421>
- Liu T, Cao P (2017) Failure mechanisms of brittle rocks under uniaxial compression. *J Theor Appl Mech* 47(3):59–80. <https://doi.org/10.1515/jtam-2017-0014>
- Liu H, Yang G, Ye W, Shen Y, Tang L (2007) Analysis of ice content and damage characteristics of frozen rock based on pseudo-color enhanced CT image. *Chin J Underground Space Eng* 10(26):2007–2013
- Liu J, Wang E, Song D, Wang S, Niu Y (2015a) Effect of rock strength on failure mode and mechanical behavior of composite samples. *Arab J Geosci* 8(7):4527–4539. <https://doi.org/10.1007/s12517-014-1574-9>
- Liu Q, Huang S, Kang Y, Liu X (2015b) A prediction model for uniaxial compressive strength of deteriorated rocks due to freeze–thaw. *Cold Reg Sci Technol* 120:96–107. <https://doi.org/10.1016/j.coldregions.2015.09.013>
- Liu H, Yuan X, Xie T (2019a) A damage model for frost heaving pressure in circular rock tunnel under freezing–thawing cycles. *Tunn Undergr Space Technol* 83:401–408. <https://doi.org/10.1016/j.tust.2018.10.012>
- Liu T, Zhang C, Zhou K, Tian Y (2019b) Freeze–thaw cycling damage evolution of additive cement mortar. *Eur J Environ Civ Eng*:1–22. <https://doi.org/10.1080/19648189.2019.1615992>
- Liu T, Zhang C, Cao P, Zhou K (2020) Freeze–thaw damage evolution of fractured rock mass using nuclear magnetic resonance technology. *Cold Reg Sci Technol* 170:102951. <https://doi.org/10.1016/j.coldregions.2019.102951>
- Martínez-Martínez J, Benavente D, Gomez-Heras M (2013) Non-linear decay of building stones during freeze–thaw weathering processes. *Constr Build Mater* 38:443–454. <https://doi.org/10.1016/j.conbuildmat.2012.07.059>
- Mimouni T, Dupray F, Laloui L (2014) Estimating the geothermal potential of heat-exchanger anchors on a cut-and-cover tunnel. *Geothermics* 51:380–387. <https://doi.org/10.1016/j.geothermics.2014.02.007>
- Özbek A (2014) Investigation of the effects of wetting–drying and freezing–thawing cycles on some physical and mechanical properties of selected ignimbrites. *Bull Eng Geol Environ* 73(2):595–609. <https://doi.org/10.1007/s10064-013-0519-y>
- Park J, Hyun C, Park H (2015) Changes in microstructure and physical properties of rocks caused by artificial freeze–thaw action. *Bull Eng Geol Environ* 74(2):555–565. <https://doi.org/10.1007/s10064-014-0630-8>
- Shen Y, Yang G, Rong T, Liu H, Lv W (2016) Proposed scheme for freeze–thaw cycle tests on rock. *Chin J Geotechn Eng* 38(10):1775–1782. <https://doi.org/10.11779/CJGE201610005>
- Tan X, Chen W, Yang J, Cao J (2011) Laboratory investigations on the mechanical properties degradation of granite under freeze–thaw cycles. *Cold Reg Sci Technol* 68(3):130–138. <https://doi.org/10.1016/j.coldregions.2011.05.007>
- Timur A (1969) Pulsed nuclear magnetic resonance studies of porosity, moveable liquid, and permeability of sandstones. *J Pet Technol* 21: 775–786
- Wang S, Zhu H, Feng X, Zhou H (2006) Influence of heterogeneity on macroscopical crack form of the brittle rock. *Rock Soil Mech* 02: 224–227. <https://doi.org/10.16285/j.rsm.2006.02.011>
- Wang C, Li J, Lin H, Liao J, Wang P, Wang S (2016a) Anisotropic mechanical characteristics of slate in uniaxial compression. *J Central South Univ (Sci Technol)* 47(11):3759–3764. <https://doi.org/10.11817/j.issn.1672-7207.2016.11.020>
- Wang P, Xu J, Liu S, Wang H, Liu S (2016b) Static and dynamic mechanical properties of sedimentary rock after freeze–thaw or thermal shock weathering. *Eng Geol* 210:148–157. <https://doi.org/10.1016/j.enggeo.2016.06.017>
- Wen L, Li X, Yin Y, Gao L (2014) Study of physico-mechanical properties of granite porphyry and limestone in slopes of open-pit metal mine under freezing–thawing cycles and their application. *J Glaciol Geocryol* 36(03):632–639. <https://doi.org/10.7522/j.issn.1000-0240.2014.0076>
- Yang G, Zhang Q, Pu Y (2003) On the microdamage characteristics of rock under the frost and thaw conditions. *J Xi'an Univ Sci Technol* 02:139–142. <https://doi.org/10.13800/j.cnki.xakjdx.2003.02.006>
- Yavuz H (2011) Effect of freeze–thaw and thermal shock weathering on the physical and mechanical properties of an andesite stone. *Bull Eng Geol Environ* 70(2):187–192. <https://doi.org/10.1007/s10064-010-0302-2>
- Zhang K, Zhang G, Hou R, Wu Y, Zhou H (2015) Stress evolution in roadway rock bolts during mining in a fully mechanized longwall face, and an evaluation of rock bolt support design. *Rock Mech Rock Eng* 48(1):333–344. <https://doi.org/10.1007/s00603-014-0546-4>
- Zhang J, Fu H, Huang Z, Wu Y, Chen W, Shi Y (2019a) Experimental study on the tensile strength and failure characteristics of transversely isotropic rocks after freeze–thaw cycles. *Cold Reg Sci Technol* 163:68–77. <https://doi.org/10.1016/j.coldregions.2019.04.006>
- Zhang G, Chen G, Jian D, Yang Y, Jiang L (2019b) Research on the freeze–thaw characteristics of rock at different temperature drop rates. *J Railway Eng Soc* 36(08):19–23 + 78
- Zhou K, Zhang Y, Li J, Xu Y (2013) Degradation mechanism and evolutionary pattern of granites with coarse and fine grains in freezing–thawing condition. *J Univ Sci Technol Beijing* 35(10):1249–1255. <https://doi.org/10.13374/j.issn1001-053x.2013.10.002>
- Zhou K, Liu T, Hu Z (2018a) Exploration of damage evolution in marble due to lateral unloading using nuclear magnetic resonance. *Eng Geol* 244:75–85. <https://doi.org/10.1016/j.enggeo.2018.08.001>
- Zhou Z, Ma W, Zhang S, Mu Y, Li G (2018b) Effect of freeze–thaw cycles in mechanical behaviors of frozen loess. *Cold Reg Sci Technol* 146:9–18. <https://doi.org/10.1016/j.coldregions.2017.11.011>